Accepted Manuscript

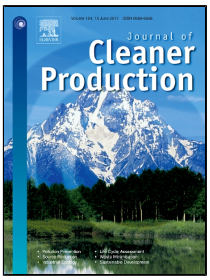

Exergy Analysis of a hydrogen and water production process by a solar-driven transcritical CO_2 power cycle with Stirling engine

Ali Naseri, Mokhtar Bidi, Mohammad H. Ahmadi, R. Saidur

PII:	S0959-6526(17)30922-8
DOI:	10.1016/j.jclepro.2017.05.005
Reference:	JCLP 9540
To appear in:	*Journal of Cleaner Production*
Received Date:	13 September 2016
Revised Date:	29 April 2017
Accepted Date:	01 May 2017

Please cite this article as: Ali Naseri, Mokhtar Bidi, Mohammad H. Ahmadi, R. Saidur, Exergy Analysis of a hydrogen and water production process by a solar-driven transcritical CO_2 power cycle with Stirling engine, *Journal of Cleaner Production* (2017), doi: 10.1016/j.jclepro.2017.05.005

- A novel cogeneration plant including Stirling engine to produce water and hydrogen.
- A dynamic RO model including recovery turbine for different permeate flow rate.
- About 8% reduction in exergy destruction in the system using ideal Stirling engine.
- More electrical power production, higher than both LNG and CO_2 power cycle.
- Electrolyzer-based ZLD approach by employing electrolyzer beside RO desalination.

Exergy Analysis of a hydrogen and water production process by a solar-driven transcritical CO_2 power cycle with Stirling engine

Ali Naseri[1], Mokhtar Bidi[1*], Mohammad H. Ahmadi[2], R. Saidur[3, 4]

1) *Faculty of Mechanical and Energy Engineering, Shahid Beheshti University, A.C., Tehran, Iran.*
2) *Department of Renewable Energies, Faculty of New Sciences and Technologies, University of Tehran, Tehran, Iran.*
3) *Research Centre for Nanomaterials and Energy Technology (RCNMET) School of Science and Technology, Sunway Universiti, No. 5, Jalan University, Bandar Sunway, 47500 Petaling Jaya, Malaysia*
4) *Department of Engineering, Lancaster University, Lancaster, LA1 4YW, UK.*

*Corresponding author. Tel.: +98 21 73932656; fax: +98 21 77311446.
E-mail address: m_bidi@sbu.ac.ir (M. Bidi).

Abstract

This study attempts to go beyond the conventional framework of the integrated solar transcritical CO_2 power cycle works, aimed at further utilization of available exergy as much as possible. This paper proposed a novel system for hydrogen and fresh water production in which a Stirling engine used instead of a condenser, for the places with abundant access to solar radiation and sea, and least to freshwater sources. This proposal leads to further utilization of streams' exergy through the system instead of wasting to the environment, and further power production by the engine followed by the higher products. The electrolyzer employed beside Reverse Osmosis (RO) desalination system, and takes full advantages of highly concentrated brine stream of desalination, eliminating the wastewater rejection through proposed system leading to attaining a near-ZLD approach in fresh water and hydrogen production. This reduces the adverse impacts of desalination's wastewater on the environment. A thermodynamic and exergy analysis is carried out to compare the superiority of this study and investigate the effect of some key parameters on the overall performance of the system as well. The results showed that replacing the condenser by a Stirling engine reduces the exergy destruction through heat transfer from CO_2 to an LNG unit. Exergy destruction was reduced from 16.7% to 8.8% for the above configuration for an ideal Stirling engine that exploits it to produce extra power which its minimum is at least 9 kW and 15 kW higher than CO_2 and LNG power productions. Moreover, Entering RO brine stream, wasting 2.58 kW exergy, to the electrolyzer leads to $NaClO$ and H_2 production besides removing brine stream. In a power plant, sodium hypochlorite is used for disinfection of cooling systems and hydrogen can be used as a source of energy in fuel cells. An examination of some thermodynamic factors showed that higher

CO_2 turbine inlet pressure has an optimum value in producing fresh water and hydrogen, while the higher CO_2 turbine inlet temperature slightly reduces the productions rate. The more recovery ratio also causes a sharp reduction in hydrogen production, whereas it has an optimum amount of fresh water production at recovery ratio equals to 0.47.

Keywords: Solar-powered transcritical CO_2; reverse osmosis; electrolyzer; LNG; Stirling engines; Zero Liquid Discharge

Nomenclature		***Greek***	
A	Area [m^2]	α	Absorbance
C_b	Bond conductance [W/mK]	β	Slope of collector [degree]
C_p	Specific heat capacity [J/kg.K]	δ	Declination angle; Thickness
D_i	Inner diameter [1]	ε	emissivity
D_o	Outer diameter [1]	η	Isentropic efficiency
Ex	Exergy [kW]	φ	Latitude [degree]
ex	Specific exergy [kJ/kg]	θ	Incident angle [degree]
F_R	Collector heat removal factor	θ_z	Zenith angle [degree]
FPC	Flat Plate Collector	π	Pi number; Osmosis pressure [kPa]
h_{fi}	Heat transfer coefficient inside the tubes [W/m^2K]	ρ	Reflectivity; Density [kg/m^3]
h	Specific enthalpy [kJ/kg]; Convective heat transfer coefficient [W/m^2K]	σ	Stefan-Boltzmann constant [$Wm^{-2}K^{-4}$]
H	Height [1]	τ	Transmittance
HT	Heater	ω	Hour angle [degree]
I	Radiation [W/m^2]; Exergy destruction [kW]	***subscript***	
k	Thermal conductivity [W/mK]	amb	Ambient
K_w	Water permeability coefficient [m^3	Aux	Auxiliary heater

	$m^{-2}s^{-1}kPa^{-1}$]		
K_T	Hourly clearance index	b	Beam; Brine water; Backside
L	Characteristic length [1]	CLT	Collector
$\dot{m}$	Mass flow [kg/s]	d	Diffuse
M	Mass [kg]	f	Feed water
N	Number of glass cover	Elz	Electrolyzer
NG	Natural Gas	g	Ground; Glass
Nu	Nusselt number	gen	Generator
P	Perimeter[l]; Pressure[MPa]; Hydraulic pressure [kPa]	i	Inlet; Insulation
PH	Preheater	load	Load
PR	Power ratio	L	Lost heat
Q	Heat [kW]	m	Membrane
r	Radius[m]	o	Outlet; Outer
R	Universal gas constant [J $mol^{-1}K^{-1}$]	P	Absorber plate; Permeate water
R_b	Beam radiation tilt factor	R	Recovery
RO	Reverse Osmosis	s	Side; Isentropic; Solar
RR	Recovery Ratio	st	Storage Tank
S	Specific entropy [kJ/kg]; Total absorbed solar radiation [W/m^2]	StE	Stirling Engine
T	Temperature [°C; K]	t	Top
TDS	Total Dissolved Solids [mg/l]	u	Useful
T_{pm}	Mean plate temperature [°C;K]	W	Wind; Water
t	Time [hour]	0	dead state
Turb	Turbine	***superscript***	
U_L	Overall loss coefficient [W/m^2K]	Chem	Chemical

V	Volume [m^3]	Electrical	Electrical work
VG	Vapor generator		
W	Tube spacing [1]; Power [kW]		
x	Water salinity [mg/l]		

1. Introduction

Utilization of low-grade thermal energy from solar radiation will be beneficial to reduce environmental impact due to burning of fossil fuels. This clean energy will also solve future energy problem. To take full advantage of this solar potential, organic and natural fluids have been used in power cycles to produce desire outputs. It is interesting to note that some of these working fluids are eco-friendly, and Carbon-dioxide is one such fluid that has promising features such as non-toxic, non-flammable, non-corrosive, the ability to reach its supercritical state at 7.38 Mpa and 31.1°C. Moreover, it has low Global Warming Potential (GWP) which is good from ecological point of view. Though utilization of transcritical carbon-dioxide power cycle empowers us to further employing low-grade heat sources, it has some limitation with its condensation temperature. Condensation process within the system just below the working fluid's critical temperature, of particular note is employing other fluids in much lower temperature to condense carbon-dioxide into its desire state and exploiting liquefied natural gas (LNG) have mostly been studied to extract the energy from power cycles [1, 2]. For further information, there have been some studies used solar units as the sources of power. *Kane et al.* [3] introduced a novel mini-hybrid solar power plant with integration of solar concentrators, superimposed with Organic Rankine Cycles and a bio-diesel engine which guaranteed a minimum level of heat and power production during the night and a few on-site tests were carried. *Boroogeni et al.* [4] proposed a bi-level control framework in order to attain a smart distribution network which uses solar panels as source of energy encompassing several residential and commercial communities with high reliability. It also dispatches the available non-renewable power plants to enhance the reliability of the communities. The results showed a theoretical low-threshold for the demand satisfaction certainty through the smart power distribution network. Moreover, there have been studies used power cycles to exploit low-grade thermal energies. *Song et al.* [5] proposed a solar-driven supercritical CO_2 power cycle with liquefied natural gas as its heat sink. In order to have a stable system output a thermal storage

tank was added and thermodynamic analysis concentrating on some key parameters in this study showed that solar radiation and condensation temperature opposite to turbine inlet temperature are the most important factors affecting net power output. *Sun et al.* [2] studied the utilization of the same transcritical power system to produce hydrogen in electrolyzer and thermodynamic and exergy analysis were carried out. Moreover, particle swarm optimization technique was used to find out the maximum exergy efficiency of hydrogen production within the system. *Xia et al.* [6] performed a thermodynamic analysis and optimization on a solar-powered transcritical power cycle with liquefied natural gas heat sink for reverse osmosis desalination and the results showed that one of the most exergy losses take places in the condenser. *Cayer et al.* [7] applied four methodologies on a carbon-dioxide power cycle with a low-grade energy of process gases as heat source. Furthermore, authors [8] performed a parametric optimization by taking some parameters including the relative cost of the system as performance pointers. *Li et al.* [9] theoretically compared and studied CO_2 transcritical power cycle and R245fa Organic Rankine cycle both with low grade heat sources. They proposed that using a recuperator in both systems would improve their exergy efficiency. A thermodynamic, exergoeconomic analysis and multi objective optimization were carried out by *Ahmadi et al.* [10, 11] on a carbon-dioxide power cycle with geothermal heat source and liquefied natural gas as heat sink. It is worthwhile to note that during recent years, some researches have been performed to use nano-fluids in power cycles. *Saadatfar et al.* [12] proposed a model of solar thermal power production system in which nano-fluids are used as working fluids in organic Rankine cycles. Moreover, some different types of nano-fluids were utilized by *Toghyani et al.* [13] in solar-powered integrated Rankine power cycle and it was revealed that any rises in volume fraction of nano-fluids leads to higher exergy efficiency. *Lin et al.* [14] proposed a novel transcritical Rankine cycle which works between exhaust from a gas turbine and liquefied natural gas as its heat source and sink. *Angelino* and *Invernizzi* [15] suggested several new schemes for the CO_2 power cycle with LNG as heat sink to utilize the cryogenic exergy of LNG and enhance the overall performance of the system. *Mehrpooya et al.* [16] proposed a hybrid system including transcritical CO_2 power cycle in a novel air separator process.

Lack of available freshwater resources to meet the demand of potable water has been one of the humans' concerns in many parts of the world, more specifically in hot and dry areas or islands in which there is a large amount of underground water or large accessibility to high seas. Moreover, abundance of renewable energy sources such as solar radiation has led to take advantage of these potentials to produce fresh water. Thus, the desalination technologies have

been developed to supply the potable water demand, Reverse Osmosis (RO) system is one of the water purification technologies that removes the large particles, ions and molecules from water by Semipermeable membranes. For further research, an onsite experimental test rig with RO desalination powered by low temperature solar organic Rankine cycle was developed by *Manolakos et al.* [17] to evaluate its performance. Experiments were conducted on Organic Rankine cycle and the small RO units to investigate their performances [18, 19]. Since employing reverse osmosis unit is the most cost-effective among the other desalination technologies, *Delgado* and *Rodriguez* [20] explored solar thermal-driven reverse osmosis desalination. Authors found it promising due to lower energy requirement to purify saline water compared to the other desalination processes driven by solar energy. *Nafey et al.* [21] studied different recovery units of a solar thermal-powered for reverse osmosis desalination system. Their thermo-economic analysis revealed that the most economic configuration in recovery of brine water stream is utilization of recovery turbine on its path. Furthermore, *Malek A. et al.* [22] studied the design and economic of RO desalinations.

When hydrogen burns, the only by-product is water and there is no harmful products entering its immediate surroundings. On the other hand, it is capable to be artificially created from sources such as methane, coal, water, gasoline, and biomass which are locally produced. Thus, these are the things that make this practical matter a clean fuel. Electrolysis, the technologies for hydrogen production which rapidly developed is the process of breaking water molecules into hydrogen and oxygen molecules in which its motive force would produce electricity in some other systems which are converted to desire direct current to drive this electrochemical process [2]. There are three types of electrolyzer, namely Polymer electrolyte membrane (PEM), alkaline water and solid oxide electrolyzer. For further research, a solar-driven transcritical CO_2 power cycle is studied by *Sun et al.* [2] to produce the hydrogen. *Dincer* [23] studied methods of hydrogen production and categorize them based on the driving sources and applications and presented various case studies to highlight the importance of green hydrogen production. *Ahmadi et al.* [24] performed energy and exergy analysis of hydrogen production by an ocean thermal energy conversion (OTEC) cycle that is coupled by a solar-enhanced PEM electrolyzer. The modeled PEM electrolyzer in this study is validated by experimental data and the parametric analysis is carried out to investigate the effect of some parameters on the system.

In addition to transcritical Rankine power cycles or Organic ones, it has been more interesting to utilize different power cycles with higher thermal efficiency and higher net power output. It is important to note that the Stirling engines not only generate higher work, but also operate

with low noise. They also produce constant power output leading to wide potential applications [25] from producing electricity with wide variety of system configurations to utilizing in regasification of liquefied natural gas. Since they produce more electricity using cold energy than using waste heat potentials at the same temperature difference for the system, *Dong et al.* [25] studied liquefied natural gas cryogenic generation with the Stirling cycle method with the seawater and LNG as its heat source. It was observed that the sink to not only gasify LNG, but also produce electrical power using Stirling cycle. *Szczygieł et al.,* and *Szargut* and *Szczygiel* [26, 27] also employed LNG cryogenic exergy-driven Stirling engine for the production of electricity without any combustion. An exergy analysis and the effect of some parameter to investigate their impacts on exergy losses also were performed. Furthermore, for high temperature heat source uses, *Ahmadi et al.* [28] used NSGA II optimization method to optimize a solar-powered high temperature differential Stirling engines using multiple criteria by developing a thermal model. The same author also performed a finite time thermo economic multi objective optimization on a solar-dish Stirling engine using the same evolutionary algorithm [29] and maximized the thermal efficiency and entransy loss rate, while the entropy generation rate was minimized both using NSGA II algorithm [30]. Moreover, finite speed thermodynamics approach [31] and non-ideal adiabatic method was used to optimize a Stirling engine. Authors also used multi objective optimization approach to design a combined Otto and Stirling cycle power plant [32].

Having highly efficient systems, more specifically in hybrid systems have captured the attentions of more scholars and there have been myriad studies aimed at further utilization of available exergy flows as much as possible. The integrated solar transcritical CO_2 power cycles also have not been exempted from this fact. However, this study attempts to go beyond the conventional framework of the transcritical power cycles by proposing a novel system using a Stirling engine instead of a condenser which is among units with highly exergy destruction within CO_2 transcritical power cycle. But, reducing exergy destruction is not the only superiority of this proposed system. Producing more power through the system from reduced destruction, comparable with summation of the total power produced throughout LNG and CO_2 power cycles, is the other merits of using Stirling engine. Moreover, having further utilization of liquid streams through the systems and reduce the liquid discharges wherever possible is one of the novel ideal notions recognized by Zero Liquid Discharge (ZLD). Employing desalination systems for producing permeate water is always accompanied by high pressure brine output with highly concentration. As it is felt a gap in applying ZLD idea to solar-driven

CO_2 transcritical power cycles, this study also attempts to approach ZLD idea in this system for producing fresh water and hydrogen by the elimination of brine output using electrolyzer. This not only reduce wastewater rejections leading to sustainable water use, but it also contributes toward taking whole advantages of water streams' exergy by generating beneficial by-products such as Hydrogen, and sodium hypochlorite.

This paper is followed by methodology of this study encompassing system description, thermodynamic model developed based on the proposed equations, the exergy analysis and the simulation conditions for the system. The third section illustrates the results of exergy and energy analysis and sensitivity analysis of some key thermodynamic parameters and the contribution of this study toward ZLD approach, and these will eventually be concluded in the last section.

2. Materials and methods

Having a general overview of this study, the following section is devoted to describe the proposed system followed by development of thermodynamic model based on some assumptions. Moreover, an exergy analysis is employed to specify destructions through the equipment due to irreversibility of systems. Finally, the simulation conditions for the system is presented to analyse the performance of the system.

2.1. System description

Figure 1 illustrates the schematic of a novel solar-driven transcritical CO_2 power cycle with recovery of cryogenic LNG using a Stirling engine. In order to model proposed novel system, the following assumptions are employed:

1. Pressure drop in all the heat exchangers within the system are 2%.
2. The Kinetic and Potential energies are neglected and all the processes are steady state.
3. The CO_2 and the LNG enter the pumps in saturated liquid state.
4. The salinity of water in electrolysis process is constant.
5. Efficiency for water electrolysis is equal to 100%.
6. Ideal conditions for Stirling engine are considered.

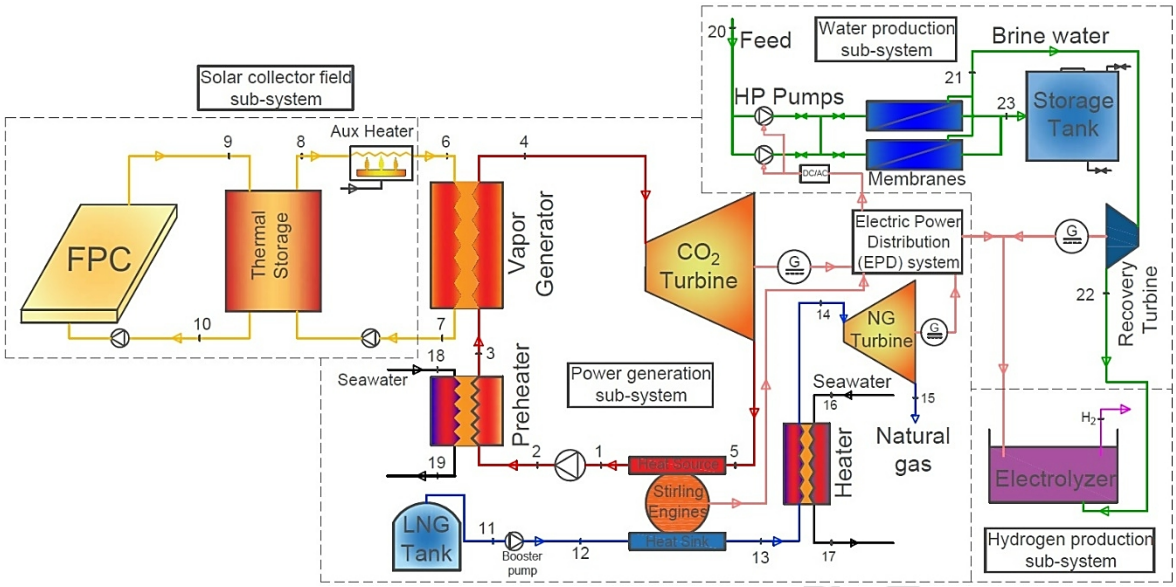

Figure 1- The schematic of proposed novel system

The model consists of solar collector field, power generation, fresh water production and hydrogen production sub-systems. The solar collector field includes two glass cover flat plate collectors to absorb solar radiation, thermal storage tank to provide stable heat and avoid any fluctuations due to sudden changes in solar radiation over the day. An auxiliary heater is used to help thermal storage tank to satisfy its minimum temperature, even at the times without sufficient irradiation [7]. Within transcritical power cycle, the temperature of CO_2 climbs in a vapor generator, and then turns into subcritical state after producing mechanical power as it goes through the turbine. At the following stage, it is condensed within a heat exchanger providing heat source for the Stirling engine. CO_2 enters into the pump in saturated liquid state and passes through a preheater to get more heat before entering the vapor generator. The Stirling engine works between two hot and cold sources that the cold one is provided by regasification of liquefied natural gas system. After pressurized in a booster pump, LNG gets heat rejected by the Stirling engine and acts as a heat sink for the engine to complete electrical power production process within the Stirling system. The heated LNG, then, enters another heater to its temperature be risen insofar as to satisfy the required temperature of the natural gas turbine. Eventually, it loses its pressure and temperature within the turbine and produces extra power for the system. The T-S diagram of the process shown in Figure 2. All the mechanical works is converted to electrical power through generators, and then it is distributed to electrolyzer and reverse osmosis sub-system with a certain ratio called “Power Ratio (PR)” that specifies the proportion of total electrical power entering the high pressure pumps of dynamic RO unit in which specified number of pressure vessels (PVs) work during the process

based on amount of electricity required to run each one. Since the brine disposal is a high pressure stream, a recovery turbine is utilized to take advantage of this beneficial stream and produce more electricity within the system. This electrical power and the amount flowing toward electrolyzer by the distribution system runs the electrolysis process through an alkaline electrolyzer with lowest cost and efficiency of about 77%. In an ideal electrolysis process without any waste heat form the reaction, the voltage equals to 1.48 V corresponding to Higher Heating Value (HHV) of reaction is needed to produce hydrogen. This voltage represents the thermo-neutral voltage of this process under the described assumption. In this paper, HHV is applied to the hydrogen production calculation. Splitting one mole of water into one mole of product needs 286 kJ of energy. Thus, one kilogram of hydrogen is produced by supplying a voltage of 1.48 V and 141.8 MJ of electricity in an alkaline electrolyzer with 100% efficiency [2].

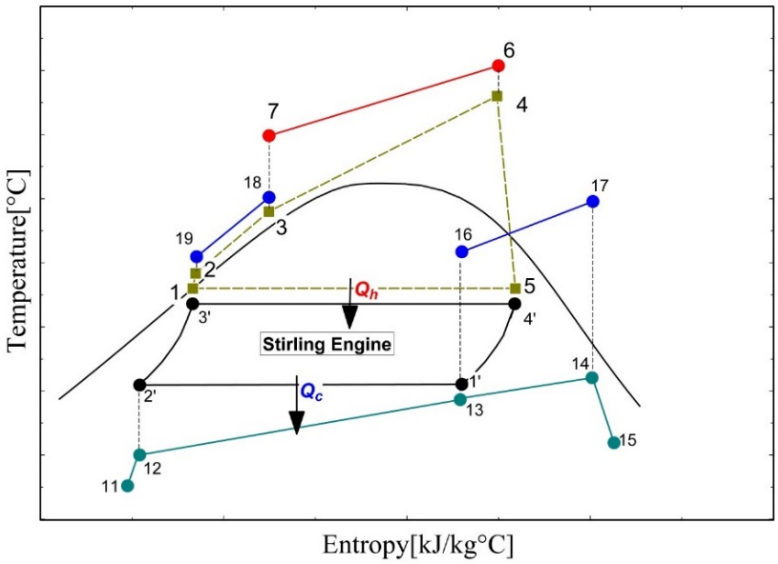

Figure 2- T-S diagram of system

2.2. System modelling

A mathematical model is developed to simulate the system at the following section and Matlab with Refprop 8.0 was used to determine fluid properties employed for this purpose [33].

2.2.1 Solar flat plate collector

Figure 3 illustrates a liquid flat plate collector with two glass covers that absorbed solar irradiation passes within these transparent covers and is absorbed by absorber plate. Then, it increases the temperature of water passing through tubes by transferring the absorbed energy

throughout tubes walls. Well insulated bottom and two sides of the solar collector prevent heat transfer to the ambient and wasting heat [35].

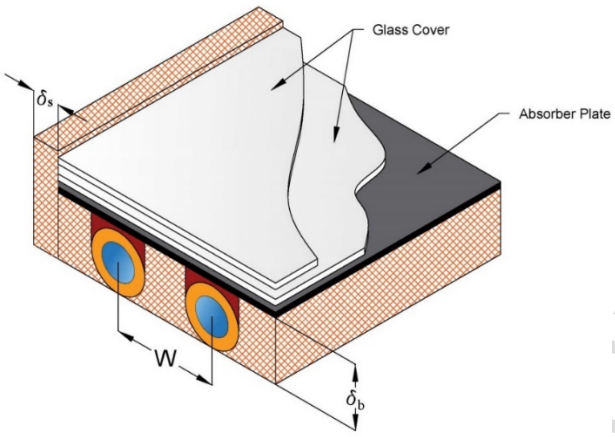

Figure 3- Liquid flat plate solar collector

The total flux absorbed by the FPC is calculated by [34]

$$S = I_b R_b (\tau\alpha)_b + I_d (\tau\alpha)_d (\frac{1+\cos\beta}{2}) + \rho_g I (\tau\alpha)_g (\frac{1-\cos\beta}{2}) \quad (1)$$

Where I_b and I_d are beam radiation and diffuse radiation, respectively. The ratio of beam radiation on a declined surface to a horizontal surface is given by,

$$R_b = \frac{\cos\theta}{\cos\theta_z} = \frac{\sin\delta\sin(\varphi-\beta)+\cos\delta\cos\omega\cos(\varphi-\beta)}{\sin\varphi\sin\delta+\cos\varphi\cos\delta\cos\omega} \quad (2)$$

In order to calculate hourly clearness index, the following equation is used.

$$K_T = \frac{I}{I_o} \quad (3)$$

The diffuse part of radiation is calculated by,

$$\frac{I_d}{I} = \begin{Bmatrix} 1.0-0.09K_T\,(K_T \le 0.22) \\ 0.9511-0.1604K_T+4.388{K_T}^2\,(0.22 \le K_T \le 0.80) \\ 0.165(0.8 \le K_T) \end{Bmatrix} \quad (4)$$

The useful heat rate gained can be calculated by,

$$Q_u = A_{CLT} F_R \left[S - U_L (T_i - T_{amb})\right] \quad (5)$$

In this equation, F_R and U_L are the heat removal factor and the overall loss coefficient. U_L includes the summation of three components as below in which U_b is the backside loss

coefficient and calculated by dividing the thermal conductivity of the insulation (k_i) to the insulation thickness (δ_b) as equation(7):

$$U_L = U_b + U_t + U_s \tag{6}$$

$$U_b = \frac{k_i}{\delta_b} \tag{7}$$

And the sides' loss coefficient is given by,

$$U_s = \frac{2k_i(a+b)c}{\delta_i ab} \tag{8}$$

Where *a*, *b* and *c* are the plate dimensions and δ_i is the thickness of sides collector insulation. An empirical equation is proposed by *Klein* [35] as follow to calculate U_t as the top loss coefficient of the collector,

$$U_t = \left[\frac{N}{\frac{C}{T_{pm}}\left[\frac{(T_{pm}-T_{amb})}{(N+f)}\right]^e + \frac{1}{h_w}}\right]^{-1} + \frac{\sigma(T_{pm}+T_{amb})(T^2{}_{pm}+T_{amb}{}^2)}{\frac{1}{\varepsilon_p + 0.00591Nh_w} + \frac{2N+f-1+0.133\varepsilon_p}{\varepsilon_g} - N} \tag{9}$$

Where *N* is the number of glass covers that is equal to 2 in this model and they improve the performance of collector and reduce the heat loss [35]. Also *f*, *c* and *e* are defined as:

$$f = (1+0.089h_w - 0.1166h_w\varepsilon_p)(1+0.07866N) \tag{10}$$

$$C = 520(1-0.000051\beta^2) \tag{11}$$

$$e = 0.430(1-100/T_{pm}) \tag{12}$$

Where h_w is wind heat transfer coefficient and can be calculated by,

$$h_w = \frac{KNu}{L} \tag{13}$$

Where

$$L = \frac{4A_{CLT}}{p_{CLT}} \tag{14}$$

In the equation (5), F_R that stands for the heat removal factor, is given by [34]:

$$F_R = F'F'' \tag{15}$$

Where

$$F' = \frac{1/U_L}{W\left[\frac{1}{U_L(D+(W-D)F)} + \frac{1}{C_b} + \frac{1}{\pi D_i h_{fi}}\right]} \tag{16}$$

$$F'' = \frac{\dot{m}\,C_p}{A_{CLT}F'U_L}\left[1-\exp\left(-\frac{A_{CLT}F'U_L}{\dot{m}\,C_p}\right)\right] \tag{17}$$

F factor is the standard fin efficiency for straight fins with a rectangular profile and is expressed as,

$$F = \frac{\tanh\left[m\left(\frac{W-D}{2}\right)\right]}{m\left(\frac{W-D}{2}\right)} \tag{18}$$

Where m is obtained from

$$m = \sqrt{\frac{U_L}{K_P\delta_P}} \tag{19}$$

In this equation, K_P and δ_P are the thermal conductivity and thickness of absorber plate, respectively.

2.2.2 Thermal storage tank and auxiliary heater

In order to have a stable heat transfer to the cycle in a vapour generator, a well-insulated thermal storage tank is employed (see Figure 4). It is assumed that the water in the tank is well-mixed and its temperature (which is assumed equals to T_{l0}) is changed uniformly throughout the time. Its heat transfer equation is as follow [36]:

$$\left[(\rho VC_p)_w + (\rho VC_p)_{\mathrm{Tank}}\right]\frac{dT_{st}}{dt} = Q_u - Q_{load} - Q_L \tag{20}$$

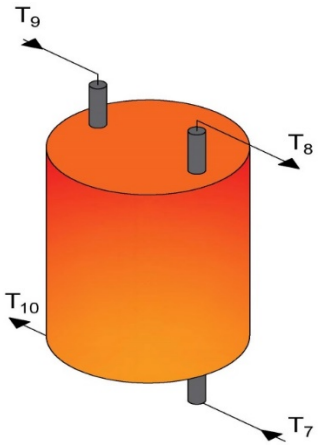

Figure 4- Well insulated thermal storage tank

In the equation (20), the useful gain, load of the system and heat loss can be defined as bellow, respectively:

$$Q_u = \dot{m}_{CLT} C_P (T_9 - T_{10}) \tag{21}$$

$$Q_{load} = \dot{m}_{load} C_P (T_8 - T_7) \tag{22}$$

$$Q_L = (UA)_{\mathrm{Tan}k} (T_{10} - T_{amb}) \tag{23}$$

And overall heat transfer coefficient of storage tank body is calculated by

$$(UA)_{\mathrm{Tan}k} = \frac{k_{ins}}{r_{i,\mathrm{Tan}k}} / (\ln(\frac{r_{O,\mathrm{Tan}k}}{r_{i,\mathrm{Tan}k}}))(2\pi r_{i,\mathrm{Tan}k} H_{\mathrm{Tan}k}) + \frac{k_{ins}}{\delta_{ins}} (2\pi r_{i,\mathrm{Tan}k}{}^2) \tag{24}$$

Also, an auxiliary heater is used to support the system heat demand throughout the day. As the outlet temperature of vapour generator in power cycle is constant, an auxiliary heater supplies the heat required in the system. This is required in case if temperature is decreases with the changes of solar radiation during the day.

2.2.3 Transcritical CO_2 power cycle

The energy and mass conservation principle is applied to each component of power cycle by considering each one as a control volume and the equations can be expressed as below.

The total heat transferred to CO_2 in vapor generator is calculated by,

$$Q_{VG} = Q_{load} = \dot{m}_{CO_2} (h_4 - h_3) \tag{25}$$

CO_2 enters a preheater before entering vapor generator and is heated by seawater. The heat transferred to the preheater is obtained from:

$$Q_{PH} = \dot{m}_{CO_2}(h_3 - h_2) \tag{26}$$

Mechanical power output of CO_2 turbine is calculated by,

$$W_{CO_2,Turb} = \dot{m}_{CO_2}(h_4 - h_5) \tag{27}$$

The efficiency of turbine is expressed as:

$$\eta_{CO_2,Turb} = \frac{h_4 - h_5}{h_4 - h_{5s}} \tag{28}$$

The total heat transfer in heat source for Stirling engine is calculated by,

$$Q_{Heat\ Source} = \dot{m}_{CO_2}(h_5 - h_1) \tag{29}$$

The CO_2 cycle pump consumption can be described as,

$$W_{CO_2,Pump} = \dot{m}_{CO_2}(h_1 - h_2) \tag{30}$$

And the efficiency of pump described as,

$$\eta_{CO_2,Pump} = \frac{h_{2s} - h_1}{h_2 - h_1} \tag{31}$$

Thus, the total net power output of CO_2 cycle is,

$$W_{CO_2,net} = W_{CO_2,Pump} + W_{CO_2,Turb} \tag{32}$$

2.2.4 Stirling engine

As it shown by T-S diagram in Figure 4, a Stirling engine works between heat source and sink with corresponding temperatures T_h and T_c .In process $1'$-$2'$, fluid compressed by piston at constant temperature and losses its heat to the heat sink and provides required heat for LNG system. In process $2'$-$3'$, fluid's temperature rises in an isochoric process, and then expands in process $3'$-$4'$ and absorbs required heat from heat source of engine, and losses heat in the isochoric process $4'$-$1'$,eventually. Therefore, for an ideal Stirling engine with an ideal fluid, the following equations are considered.

$$Q_{c,StE} = mRT_c \ln\left(\frac{V_{\min}}{V_{\max}}\right) = \dot{m}_{LNG}(h_{13} - h_{12}) \tag{33}$$

$$Q_{h,StE} = mRT_h \ln\left(\frac{V_{\min}}{V_{\max}}\right) = \dot{m}_{CO_2}(h_5 - h_1) \tag{34}$$

$$W_{StE,net} = mR(T_h - T_c)\ln(V_{\max}/V_{\min}) \tag{35}$$

$$\eta_{StE} = \frac{W_{StE,net}}{Q_{h,StE}} = \frac{T_h - T_c}{T_h} = 1 - (T_C/T_h) \tag{36}$$

It is obvious that thermal efficiency of a Stirling engine is exactly equal to its Carnot efficiency [37].

2.2.5 LNG evaporation

The saturated LNG at ambient pressure is pumped by a booster pump to the heat sink of the Stirling engine and turning into a gas mixture by absorbing rejected heat. Thus, by applying the energy and mass conservation principle, the equations can be expressed as below.

The pump's net power consumption is calculated by

$$W_{LNG,Pump} = \dot{m}_{LNG}(h_{11} - h_{12}) \tag{37}$$

And its efficiency is,

$$\eta_{LNG,Pump} = \frac{h_{12,s} - h_{11}}{h_{12} - h_{11}} \tag{38}$$

Ejected natural gas from the Stirling heat sink is more heated by seawater in a heater that its heat transfer equation is,

$$Q_{HT} = \dot{m}_{LNG}(h_{14} - h_{13}) \tag{39}$$

Net output power of NG turbine is expressed by

$$W_{NG,Turb} = \dot{m}_{LNG}(h_{14} - h_{15}) \tag{40}$$

And the efficiency of turbine is

$$\eta_{NG,Turb} = \frac{h_{14} - h_{15,s}}{h_{14} - h_{15}} \tag{41}$$

Thus, the net mechanical power output of LNG sub-system is calculated by

$$W_{LNG,net} = W_{NG,Turb} + W_{LNG,Pump} \tag{42}$$

2.2.6 Reverse osmosis desalination and recovery configuration

The RO unit consists of pressure vessels (PVs) that are fed by high pressure pumps. Each PV includes some semipermeable membranes preventing the large particles, ions and molecules to

pass through them. The number of pressure vessels operating in RO unit could vary proportion to the power entering the RO high pressure pumps and consequently the fresh water production could be changed. Due to the high impurity of seawater, one stage of PVs is used usually and the number of passes could vary by Total Dissolved Solids (TDS) that is expected in permeate water. One of the main parameter in RO unit is Recovery Ratio (RR) that presents the percentage of the feed water which becomes product water. Thus, a RO unit with Recovery Ratio (RR) of 0.3, one pass and one stage with constant temperature of water equal to inlet feed water and specified membrane type is considered in this model and the mass and salt balance of RO is expressed as below [38]

$$\dot{m}_f = \dot{m}_P + \dot{m}_b \tag{43}$$

$$\dot{m}_f x_f = \dot{m}_P x_P + \dot{m}_b x_b \tag{44}$$

Where $\dot{m}_f$, $\dot{m}_P$ and $\dot{m}_b$ are the feed water, permeate water and brine water flow rate respectively. Also, x_f, x_P and x_b are the salinity of feed water, permeate water and brine water. Then, the mass flow rate of feed water is calculated by,

$$\dot{m}_f = \frac{\dot{m}_P}{RR} \tag{45}$$

Osmotic pressure of flows can be expressed by

$$\pi_f = RTx_f \tag{46}$$

$$\pi_P = RTx_P \tag{47}$$

$$\pi_b = RTx_b \tag{48}$$

Where R is universal constant of gases and T is the temperature of the flows. So, the total osmotic pressure of system can be obtained from:

$$\Delta\pi = \left(\frac{\pi_f + \pi_b}{2}\right) - \pi_P \tag{49}$$

By knowing the salinity and temperature of brine water, the water permeability coefficient can be calculated by

$$K_w = \frac{6.84\times10^{-8}\times\left[18.68-(0.177\times x_b)\right]}{T_f} \tag{50}$$

And permeate hydraulic pressure is obtained from

$$\Delta P = \frac{\dot{m}_P}{K_w A_m} + \Delta\pi \tag{51}$$

Totally, net power consumption of high pressure pumps can be calculated by

$$W_{RO,net} = \frac{\Delta P_{net}\dot{m}_f}{\rho_f \eta_{RO,Pump}} = PR(W_{LNG,net} + W_{CO_2,net}) \tag{52}$$

Where, ρ_f, $\eta_{RO,Pump}$ and ΔP_{net} are the feed flow density, the mechanical efficiency of RO pumps and the net pressure difference across the pumping process. There are different configurations to recover the energy of high pressure brine water. The considered configuration in this paper is using a Pelton wheel turbine in the brine water outlet of RO system. Thus, mechanical work will be produced by decreasing the pressure of brine water [21]. In other word, the power consumed in RO high pressure pumps to rise up pressure of feed water, could be recovered by this recovery turbine. The net output power of the recovery turbine is calculated by,

$$W_{R,Turb} = \dot{m}_b(h_{21} - h_{22}) \tag{53}$$

2.3. Exergy analysis of streams

Exergy is the maximum theoretical useful work obtained when a system only interacts with the reference environment to bring it into thermodynamic equilibrium state. One of the applications of exergy is to specify the exergy destruction in the equipment due to irreversibility of systems. The physical exergy of each stream can be calculated by [39]:

$$ex_i = (h_i - h_0) - T_0(s_i - s_0) \tag{54}$$

Exergy balance should be written to compute exergy destruction (*I*) in each component and by applying the first and second laws of thermodynamics, it can be written as follows [39]:

$$\sum_i \dot{m}_i\, ex_i + Ex_{Q_i} = \sum_e \dot{m}_e\, ex_e + Ex_{Q_e} + Ex_W + I \tag{55}$$

In this equation, the subscripts *i* and *e* stand for the inlet and outlet of the control volume. In order to calculate chemical exergy of the fuel which is burnt in the auxiliary heater, the following equation can be used [41]:

$$\xi = \frac{ex^{Chem}{}_f}{LHV_f} \tag{56}$$

The ratio of chemical exergy of fuel to lower heating value of the fuel for Methane (CH_4) and hydrogen (H_2) are equal to 1.06 and 0.985[39]. The exergy destruction equations for system components are shown in Table 1, while $W_{net,cycles}^{electrical}$ is calculates by equation (58). Also, the solar radiation exergy absorbs by the collector is calculated by [41]:

$$Ex_{solar} = Q_{Solar}\left[1+\frac{1}{3}\left(\frac{T_0}{T_s}\right)^4 - \frac{4}{3}\left(\frac{T_0}{T_s}\right)\right] \quad (57)$$

$$W_{net,cycles}^{electrical} = \eta_{gen} \times W_{net,CO_2} + \eta_{gen} \times W_{net,LNG} \quad (58)$$

Where Q_{Solar} is heat absorbed by the collector and *Ts* is the temperature of solar radiation.

Table 1- Expression for exergy destruction of the novel co-generation modeled system.

$I_{CLT} = Ex_{solar} - (Ex_9 - Ex_{10})$	$I_{NG,Turb} = (Ex_{14} - Ex_{15}) - W_{NG,Turb}$
$I_{Aux} = Ex_f^{Chem} - (Ex_6 - Ex_8)$	$I_{LNG,Pump} = W_{LNG,Pump} - (Ex_{12} - Ex_{11})$
$I_{st} = (Ex_9 - Ex_{10}) - (Ex_8 - Ex_7)$ $-Ex_{L,st} - Ex_{Store}$	$I_{LNG,HT} = (Ex_{16} - Ex_{17}) - (Ex_{14} - Ex_{13})$
$I_{CO_2,VG} = (Ex_6 - Ex_7) - (Ex_4 - Ex_3)$	$I_{Elz} = (1-PR)(W_{net,cycles}^{electrical} + W_{StE}) + W_{R,Turb} - Ex_{H_2}$
$I_{CO_2,Turb} = (Ex_4 - Ex_5) - W_{CO_2,Turb}$	$I_{RO} = PR\,(W_{net,cycles}^{electrical}) - (Ex_{23} + Ex_{21} - Ex_{20})$
$I_{CO_2,Pump} = W_{CO_2,Pump} - (Ex_2 - Ex_1)$	$I_{R,Turb} = (Ex_{21} - Ex_{22}) - W_{R,Turb}$
$I_{CO_2,PH} = (Ex_{18} - Ex_{19}) - (Ex_3 - Ex_2)$	$I_{gen} = W_{inlet} - W_{outlet}^{electrical}$
$I_{StE} = (Ex_5 - Ex_1) - (Ex_{13} - Ex_{12}) - W_{StE}$	

2.4. Simulation conditions for the system

In order to analyse the performance of the model, a numerical simulation is carried out based on the data of Boushehr province in Iran and 15 May [42]. Table 2 shows simulation conditions at a glance.

Table 2-Simulation condition for the system

Parameter	Unit (SI)	Value
Environment pressure	kPa	101.325
Inner diameter of the absorber tube	mm	14

Specific heat capacity of water	J/kg.K	4,195
Total surface of absorber plate	m^2	384
Specific heat capacity of steel tank	J/kg.K	460
Tube Spacing	mm	15
Inner diameter of storage tank	m	1.7
Height of storage tank	m	4.2
Number of thermal storage tanks	-	4
CO_2 turbine inlet pressure	MPa	10
CO_2 turbine inlet temperature	°C	65
CO_2 turbine isentropic efficiency	%	70
Condensation temperature	°C	-10
CO_2 Pump isentropic efficiency	%	80
Pinch point temperature difference at vapor generator	°C	10
Pinch point temperature difference at Stirling engine heat sink	°C	5
Pressure drop in heat exchangers	%	2
LNG tank temperature	°C	-161.47
LNG tank pressure	kPa	101.43
LNG working pressure	MPa	6.3175
LNG pump isentropic efficiency	%	70
NG turbine isentropic efficiency	%	80
NG turbine inlet temperature	°C	10
NG turbine outlet pressure	MPa	4.00
RO feed water TDS	mg/l	35,612
Warm sea water temperature	°C	298.15
RO feed water temperature	°C	25.0

RO permeate water pressure	kPa	101.35
Recovery Ratio, RR	-	0.3
RO pumps inlet pressure	kPa	101.35
RO pumps isentropic efficiency	%	80
RO membrane typical flux	gfd	10
Membrane in each pressure vessel	-	6
Recovery turbine outlet pressure	kPa	303
Recovery turbine isentropic efficiency	%	80
Heater and preheater hot side temperature drop	°C	20
Generators efficiency	%	95

3. Results and discussion

3.1. Exergy analysis and performance criteria

Figure 5 illustrates overall performance of the system over a period of 24-hour. Generally, it can be seen that the useful heat gain through solar flat plate collectors which is calculated by equation (5) reaches a peak at the middle of the day at 11:00, while its value declines over the off-peak hours up to the minimum value equals to zero due to insufficient sun light. Consequently, the required heat amount entering power cycle (based on equation (22)) would alter during the day and thermal storage tank and auxiliary heater is essentially uses to overcome this variation to have a stable system output. In other words, they provide the minimum requirements for the cycle to run continuously. Moreover, the figure shows changing temperature through thermal storage tank (T_{10}) based on equation (20) and temperature of heat transfer fluid leaving collectors (T_9). Due to not only lack of solar radiation, but also to provide required heat for system, during the first and last 8-hour over a day, thermal storage tank's temperature falls, while it moderately rises simultaneously as sufficient heat is absorbed by collectors.

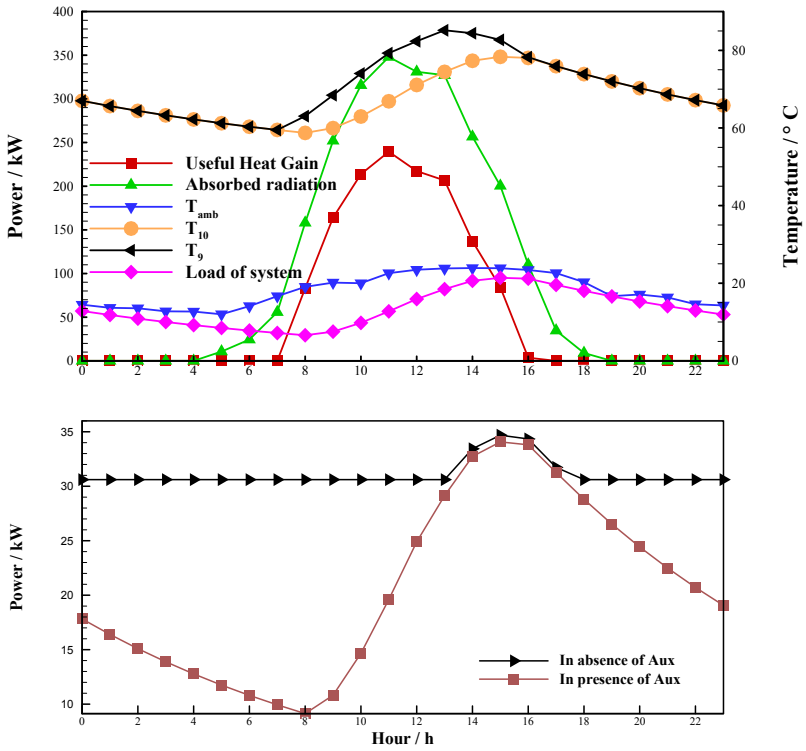

Figure 5-Overall performance of the system

It is noteworthy that over the times without any irradiations, the water is stopped circulating within the FPC system. Insofar as the pinch condition within the vapor generator is satisfied, the system works without any extra heat, otherwise, the auxiliary heater should provide the required heat to have a continuous system output. In order to compare the system performance in absence and presence of heater, Figure 5 illustrates the importance of the auxiliary heater attendance in variation of total system output mechanical power. In the absence of the auxiliary heater, the system experiences fluctuation by about 25 kW, while the heater helps the system to meet its minimum heat requirement to satisfy pinch condition in VG.

To perform thermodynamic and exergy analysis, the time corresponding to the maximum load of system based on Figure 5 is chosen (in this study it equals to 15:00). Furthermore, power ratio (PR) corresponding to the amount of permeate water and hydrogen production is arbitrarily chosen as 0.65 just to calculate the production rate for system. As a result, the following Table 3 shows the thermodynamic parameter of system at each node.

Table 3-system nodes' thermodynamic characteristics

State	T(℃)	P(MPa)	h(kJ/kg)	s(kJ/kg)	ex(kJ/kg)	m(kg/s)
1	-10.000	2.649	176.530	0.916	213.638	0.484
2	-4.183	10.412	186.403	0.923	221.236	0.484

3	20.000	10.204	242.358	1.123	217.645	0.484
4	65.000	10.000	438.823	1.746	228.496	0.484
5	-9.298	2.702	408.533	1.795	183.538	0.484
6	78.333	0.101	328.063	1.056	17.868	0.800
7	50.000	0.101	209.418	0.704	4.151	0.800
8	78.333	0.101	328.063	1.056	17.868	0.800
9	82.696	0.101	346.376	1.107	20.742	4.600
10	78.333	0.101	328.063	1.056	17.868	4.600
11	-161.470	0.101	0.044	0.000	1079.966	0.169
12	-157.896	6.578	21.860	0.058	1084.710	0.169
13	-59.298	6.446	560.915	3.216	682.006	0.169
14	10.000	6.317	806.364	4.236	623.513	0.169
15	-17.865	4.000	762.270	4.279	566.438	0.169
16	25.000	0.101	104.920	0.367	0.000	0.496
17	5.000	0.099	21.118	0.076	2.944	0.496
18	25.000	0.101	104.920	0.367	0.000	0.323
19	5.000	0.099	21.118	0.076	2.944	0.323
20	25.000	0.101	104.920	0.367	0.000	3.290
21	25.000	5.179	109.668	0.366	5.148	2.329
22	25.000	0.300	106.017	0.367	1.112	2.329
23	25.000	0.101	104.920	0.367	0	0.962

In the corresponding time of the day, some inputs, consumptions and outputs of system is illustrated by Table 4. It is obvious that a large number of input exergy through LNG tank or collectors destructs through the system (see Table 5), calculated by equations in Table 1. It mostly destructs by solar collectors and then Stirling engine with 173.899 kW and 32.563 kW, respectively.

Table 4- Some system parameters relating input, consumptions and outputs

Term	Value	Unit
Solar exergy	187.122	kW
LNG exergy	182.814	kW
CO_2 Turbine power	14.660	kW
CO_2 pump power	4.778	kW
LNG Turbine power	7.464	kW
LNG Pump power	3.693	kW
Stirling engine power	21.037	kW
Recovery turbine power	8.505	kW
RO pump power consumption	20.421	kW
Hydrogen production rate	1.309	l/s
Permeate production rate	0.964	l/s

Table 5-Exergy destruction within the system

Units	Exergy destruction(kW)
Solar collector	173.899
Thermal Storage tank	2.249
Vapor Generator	5.721
CO_2 turbine	7.100
CO_2 pump	1.101
Stirling Engine	32.563
Preheater	0.787
LNG turbine	2.197
LNG pump	2.890
Heater	8.442
RO desalination unit	8.432
Recovery turbine	0.894
Electrolyzer	4.984
CO_2/LNG/Recovery Generators	0.494/ 0.188/0.425

3.2. Exergy flow throughout the system and a comparison

Consider the conventional system with condenser in which the stream 5-1 condensates in contact with LNG within the condenser as what Xia [6] proposed in his model. So, the exergy destruction equation would be as below:

$$I_{Condenser} = (Ex_5 - Ex_1) - (Ex_{13} - Ex_{12}) \quad (59)$$

The differences between this equation and exergy destruction in a Stirling engine equation is the produced power within the process through the engine and the mass flow rate of LNG unit which measures by equation (33). Thus, the exergy destruction in heat that flows through the condensation process of CO_2 to the heating process of LNG reduces due to employing a Stirling engine. Totally, the exergy destruction of system interestingly decreases.

Table 6 depicts the exergy flow throughout the system either by the condenser and Stirling engine based on equations in Table 1 and streams exergy calculated by equation (54). As it can be seen, the exergy destruction through the Stirling engine is just 8.802% of total input exergy considering ideal conditions for the Stirling engine, while this value for the conventional

condenser system is about 16.712%. It has to be noted that the calculations for conventional system is in the same condition as this novel proposed model. Thus, the exergy destruction through heat transfer from CO_2 to an LNG unit decreases by approximately half and this shows the advantage of using Stirling engine instead of condenser. The reduced exergy destruction is also about 36.54 kW which Stirling engine exploits it to produce extra power. Based on Table 4, the ideal Stirling engine provides 21.037kW electrical power, while there is no output power through the condenser in conventional systems. As a result, it provides more input power for the RO desalination unit and Electrolyzer one and helps the system with more production rate. It is fair to say that the exergy output of stream number 15 corresponding with the natural gas turbine output stream decreases due to a reduction in the LNG mass flow rate of the modelled system leading to lower heat transfer area within the LNG heater. This also causes lower exergy destructions through the equipment in LNG power system.

Table 6-Exergy flow throughout the system

Term		Presence of Stirling Engine		Presence of Condenser	
		Value(kW)	Percentage (%)	Value(kW)	Percentage (%)
Exergy input	Solar	187.122	50.582	187.122	45.501
	LNG	182.814	49.418	224.127	54.499
Exergy losses	Vapor Generator	5.721	1.547	5.722	1.384
	CO_2 turbine	7.100	1.919	7.223	1.747
	Stirling Engine/ (Condenser)	32.563	8.802	69.102	16.712
	CO_2 pump	1.101	0.298	1.101	0.266
	Preheater	0.787	0.213	0.786	0.190
	Electrolyzer	4.984	1.347	1.949	0.471
	Solar collector	173.899	47.008	173.899	42.058
	LNG turbine	2.197	0.594	2.693	0.651
	LNG pump	2.890	0.781	3.541	0.857
	Heater	8.442	2.282	9.882	2.390
	RO desalination	8.432	2.279	3.739	0.904
	Recovery turbine	0.894	0.242	1.336	0.323
	Generators	1.108	0.299	0.924	0.223
	Storage Tank	2.249	0.608	2.252	0.544
Exergy output	NG turbine outlet	95.886	25.919	117.603	28.443
	Permeate water outlet	0.00	0.000	0.000	0.000
	Brine water outlet	2.590	0.700	0.247	0.598
	Produced H_2	16.682	4.509	6.522	1.577
	Stream no.19	0.951	0.257	0.952	0.230
	Stream no.17	1.460	0.395	1.781	0.431

3.3. Performance analysis of the system

Figure 6 depicts the variation of power generation by Stirling engine, CO_2 and LNG power cycles. It is obvious that the idea Stirling engine produce more power than CO_2 and LNG power cycles so that the minimum power produced by Stirling engine is noticeably at least 9 kW and 15 kW higher than CO_2 and LNG power productions. In other words, it produces more than summation of power cycle's electricity generation due to

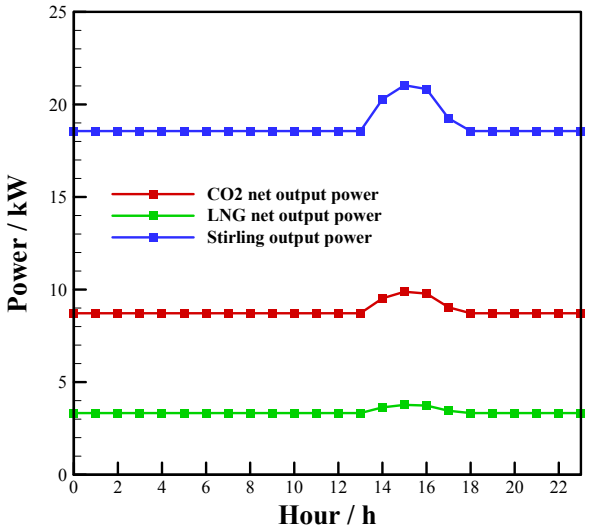

Figure 6- Power generation within the system

In terms of peaks in this figure it is fair to say that daily solar radiation changes lead to changes in mass flow rate of CO_2 in power cycle. Due to presence of auxiliary heater it remains unchanged during hours without sufficient radiation at which the heater help system with satisfying the minimum temperature requirement in vapour generator by adding extra heat to system. As the hours go on, the collector absorbs sunlight energy and CO_2 mass flow rate reaches a peak. Then, it moderately decreases to it minimum. Figure 7 presents variation of mass flow rate with pressure for the CO_2 power cycle. As the turbine inlet pressure is increased, working fluid's mass flow rate is increased. This happens as the vapour generator outlet pressure increases, the enthalpy of CO_2 decreases. Therefore, for the same heat transfer through vapour generator, more CO_2 needs to be flowed to carry the same heat. The reason for the fluctuations in this figure is also due to changes in mass flow rate of CO_2 in power cycle as it is discussed above.

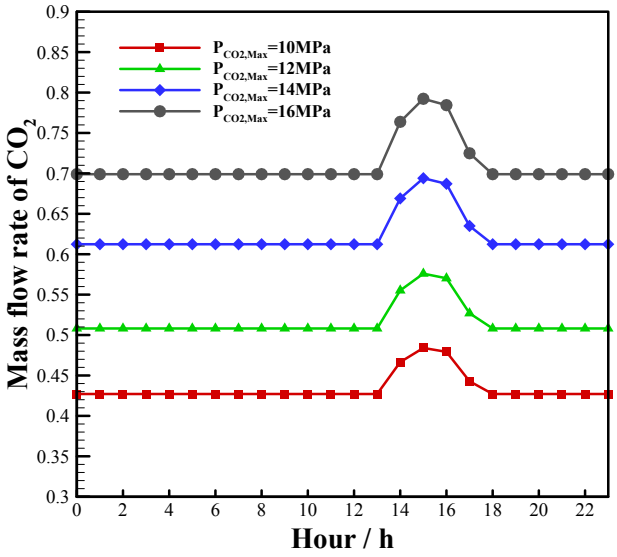

Figure 7-CO_2 mass flow rate variation versus daily hours

As it is mentioned above, the power ratio shows the ratio of total generated power entering the desalination unit to electrolyzer one. Meanwhile, a recovery turbine is utilized in outlet brine stream of desalination system due to its little pressure difference with feed water entering pressure vessels. So, this high pressure stream produces more power for electrolyzer employing a percentage of total power produced by power cycles and Stirling engine. Figure 8 illustrates hydrogen and permeate water mass flow rate on a daily basis. Fresh water and hydrogen productions remains constant in off-peak times, while it reaches a peak at 15:00 due to maximum power generation by cycles and Stirling engine because of high solar radiation and maximum accumulated energy within the thermal storage tank at that time, while in the off-peak times auxiliary heater just provides the required energy for the system as shown in Figure 5.

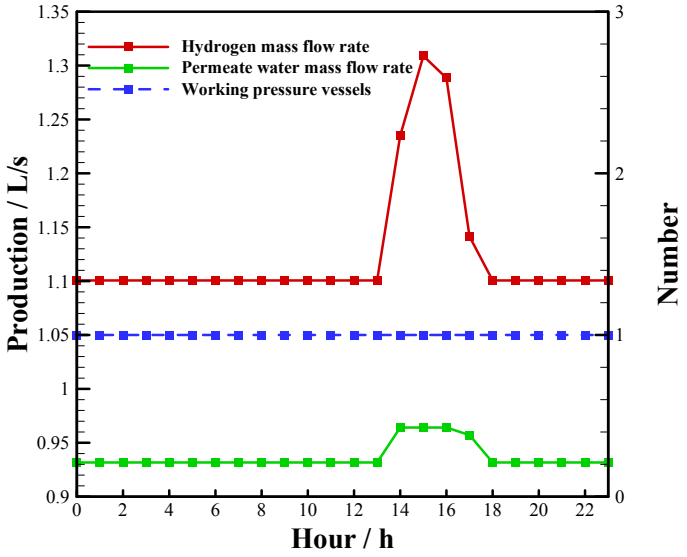

Figure 8-Permeate water and hydrogen production changes and active pressure vessels

As a specified number of pressure vessels works based on total power entering RO high pressure pumps in a fixed typical flux of membranes, the active pressure vessels varies through the unit. The range of power entering desalination system in this model is just able to activate one pressure vessel as shown in Figure 8.

3.4. Effect of CO_2 turbine inlet pressure

Figure 9 and Figure 10 compare the effect of CO_2 turbine inlet pressure on both power cycles' parameters and permeate water and hydrogen production rate. It can be seen that CO_2 cycle's net output power increases sharply, and falls noticeably after reaching a peak, though CO_2 mass flow rate climbs continuously. This is because the pump consumed power overweighs turbine produced power. Hence, either hydrogen and permeate water production rate follow the net power output of CO_2 power cycle. As is illustrated by Figure 10, the more inlet pressure through the CO_2 turbine brings about less enthalpy difference between inlet and outlet of the Stirling engine heat source, while CO_2 mass flow rate increases. Firstly, drop in enthalpy difference overweighs any rises in CO_2 mass flow rate and then it happens reversely. So, LNG mass flow rate and LNG net power output witness a fall to reach their minimum and then climb remarkably. It has to be noted that the variation of CO_2 net power output prevails the LNG one's which enforces tracking its trend on production rates. Figure 11 shows the variation of Stirling output power versus the variation of turbine inlet power. As the same reason, the trend is as same as what happens for LNG power cycle.

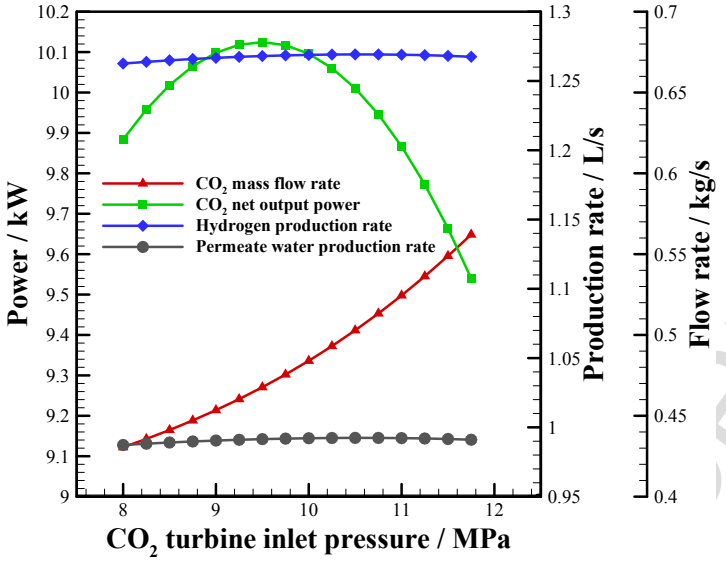

Figure 9-Effect of CO_2 turbine inlet pressure on CO_2 net output power and mass flow rate, hydrogen and permeate water production rate

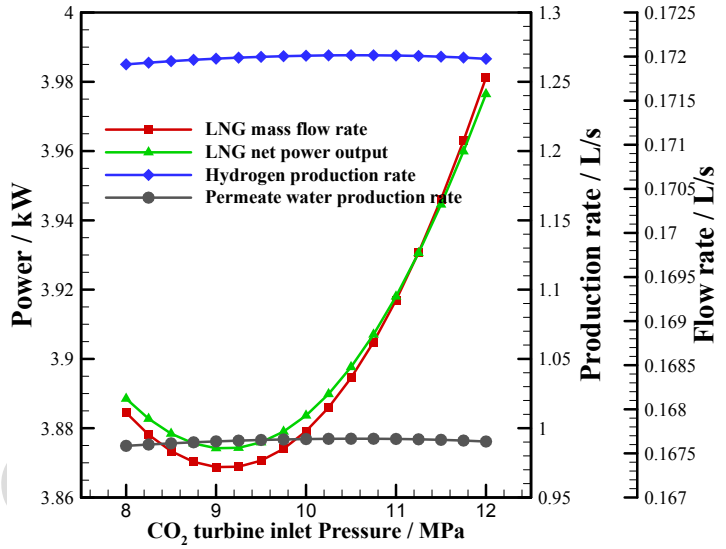

Figure 10- Effect of CO_2 turbine inlet pressure on LNG net output power and mass flow rate, hydrogen and permeate water production rate

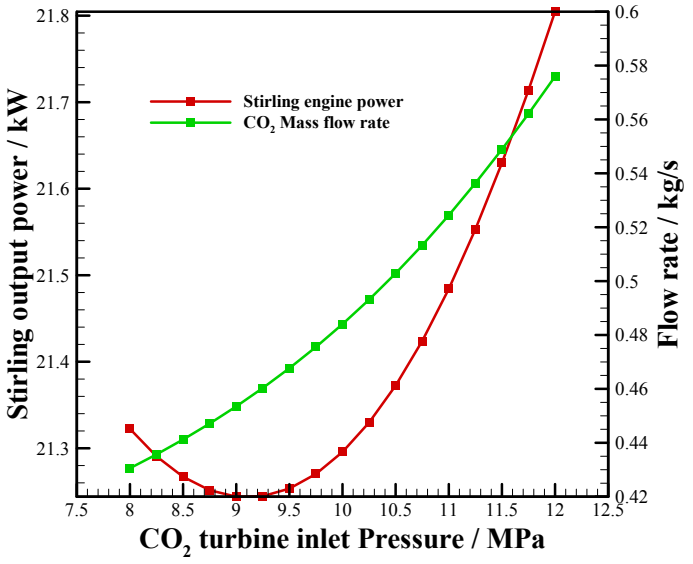

Figure 11- Effect of CO_2 turbine inlet pressure on Stirling engine power output

3.5. Effect of CO_2 turbine inlet temperature

One of the main parameters affecting net power output of system is the turbine inlet temperature. As the temperature of point 4 representing the turbine inlet temperature in T-S diagram illustrated in Figure 2 climbs, the enthalpy difference between VG inlet and outlet increases that causes a sharp fall in CO_2 mass flow rate through the system. However, length of stream 4-5 that shows the turbine power output increases and totally CO_2 net power output increases. Figure 12 depicts this variation and its effect on CO_2 and total net output power, CO_2 mass flow rate and the hydrogen and fresh water production rate. The same also holds true for the LNG power cycle. Any reduction in CO_2 power cycle leads to less heat rate transferring by heat source of Stirling engine and not only reduces the Stirling engine power output (see Figure 13), but it also affect the heat rejected to LNG power cycle which cause a noticeably reduction in LNG mass flow rate. Although the reduction of LNG mass flow rate decreases both pump consumption and turbine power production, the mass flow rate reduction rate is descending. It means that as the CO_2 turbine inlet temperature increases, the difference of reduction in each interval of LNG mass flow rate reduces that leads to descending reduction rate in pump and turbine net power. So, the net power output of LNG sub-system increases. Eventually, the total net power output including CO_2 and LNG cycles' net power output and Stirling engine falls moderately (see Figure 12) and the fresh water and hydrogen production rate decreases.

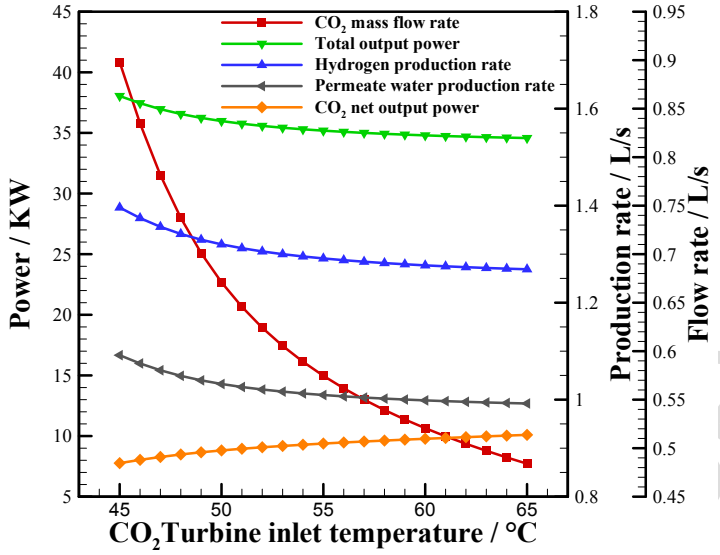

Figure 12- Effect of CO_2 turbine inlet temperature on net output power, CO_2 mass flow rate, hydrogen and permeate water production rate

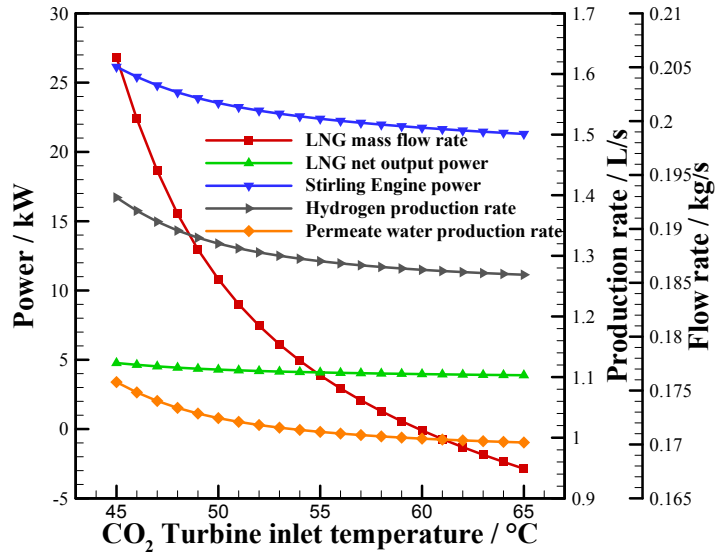

Figure 13-Effect of CO_2 turbine inlet temperature on LNG net output power, LNG mass flow rate, Stirling engine power output and hydrogen and permeate water production rate

3.6. Effect of VG inlet temperature

Figure 14 shows the variation of CO_2 and LNG cycles' net power output, the Stirling engine power production, and RO desalination and electrolyzer productions. The increase in vapour generator inlet temperature in cold side (CO_2 side's vapour generator temperature) in constant heat transfer from cold side of the vapour generator causes more mass flow rate due to reduction in enthalpy difference between vapour generator's cold side inlet and outlet that increases total

net power output of CO_2 power cycle. The higher mass flow rate in CO_2 power cycle means higher heat transfer through heat source and sink of Stirling engines. So, the Stirling and LNG net output power increases and the system's productions rate rises smoothly.

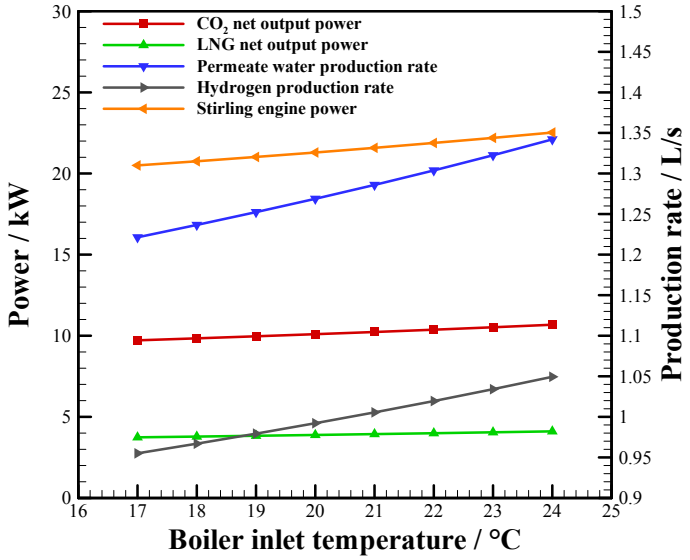

Figure 14-Effect of VG inlet temperature on net output power of cycles and production rate of hydrogen and permeate water

3.7. Effect of NG turbine inlet pressure

The other parameter affecting LNG sub-system power output is the LNG pressure at the inlet of the NG turbine. The more pressure cause more enthalpy difference between inlet and outlet of turbine leading to more power output for the system which is illustrated by Figure 15. Thus, the total net output power rises leading to produce more permeate water and hydrogen.

3.8. Effect of recovery ratio

The key factor that affects the fresh water and hydrogen production rate is recovery factor which is the ratio of distilled water produced to feed water flow rate. In other words, a part of feed water flows through RO membranes and is desalinated, while the remaining saline solution is rejected by pressure vessels. Therefore, the higher recovery ratio causes more fresh water production and less brine stream reducing the mass flow rate of stream entering recovery turbine. Thus, the power production of recovery turbine decreases (see Figure 16). Since, the total power entering electrolyzer includes the fraction of system's net output power and the entire recovery turbine produced power, less hydrogen would produce. Meanwhile, in the

specified design parameters of RO desalination system, a specified maximum amount of feed water would be desalinated. As a result, the permeate water production rate peaks at a specified recovery ratio of 0.47 and then decreases.

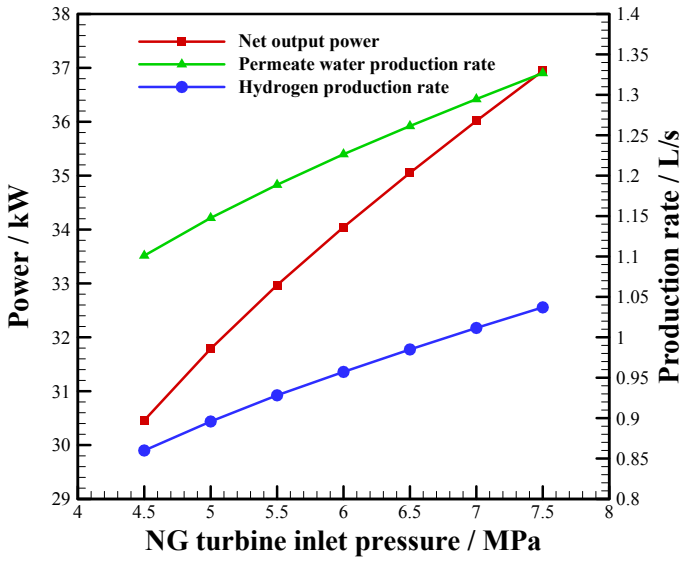

Figure 15-Effect of NG turbine inlet pressure on total net output power and production rate of hydrogen and permeate water

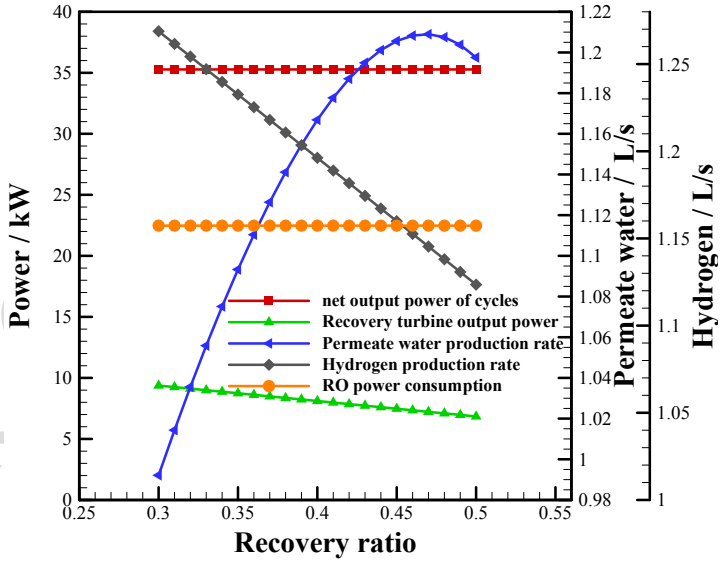

Figure 16-Effect of recovery ratio on total net output power, production rate of hydrogen and permeate water, RO pump consumption and recovery turbine power output

3.9. Electrolyzer based Zero Liquid Discharge (ZLD) approach

One of the main aims of this study, and cooperation of RO desalination and electrolysis system is approaching the zero liquid discharge (ZLD) idea in which the whole advantages of probable liquid discharges is taken place. Wastewaters produced through some industrial plants might be followed by adverse impacts on humans' life or flora and fauna. So, treating and recovering these streams are among the ways to not only eliminate these minus effects, but it also contributes to sustainable water use leading to zero liquid discharge. This ideal notion states all the water cycles within the system should be closed so as to remove any discharge from the system to minimize the amount of required water for the system and exploit recycled discharge streams wherever possible [43]. There are different ZLD approaches, the most common method is a combination of evaporator and crystallizer to convert rejected waste waters to demineralized water and solid salt. But, here we are introducing a new approach concerning electrolysis of rejected brines to produce sodium hypochlorite and hydrogen. In a power plant sodium hypochlorite is used for disinfection of cooling systems and hydrogen can be used as a source of energy in fuel cells. In this case, employing electrolyzer beside desalination system in order to use highly concentrated brine stream of RO system would remove the wastewater rejection through this proposed system (as shown in Figure 17).

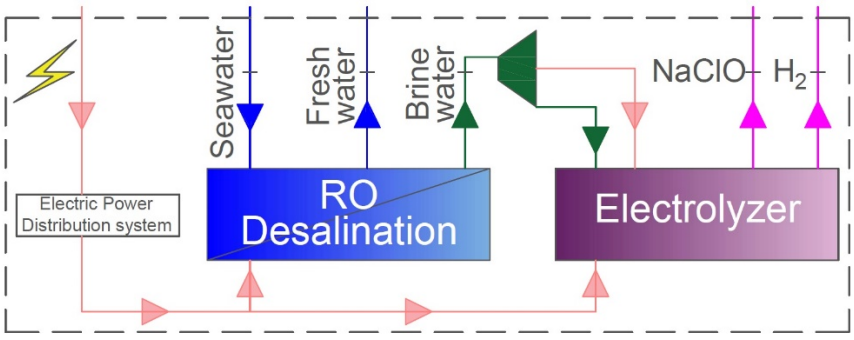

Figure 17 – Electrolyzer based ZLD approach applied on water and hydrogen production part of the proposed system.

As it mentioned above, the high pressure brine is passed through recovery turbine to produce extra water, while brine concentration remains constant. So, using an electrolyzer through which this concentrated salt water turns into beneficial products eliminates water rejection in the system and this would be an effective step to achieve a near-ZLD system. One of the well-

known systems is Sodium Hypochlorite Generators (SHG) that produce hydrogen and sodium hypochlorite through the electrolysis process as follow [42]:

$$NaCl + H_2O + electricity \rightarrow NaClO + H_2 \quad (60)$$

Applying the ZLD approach in this study, the brine with about 50000 ppm concentration and 8.6 kg/s mass flow rate rejected from desalination system (at the time corresponding to the maximum load of the system) enters electrolyzer which is supplied by power distribution system. Thus, in the water and hydrogen production part of the system it is witnessed omitting brine stream by which 2.58 kW of inlet exergy is wasted based on Table 6. This means that the system produce permeate water through desalination system and *NaClO* and H_2 through electrolysis system without any waste liquid rejection in the system and this leads to attain a near-ZLD approach. In as much as the proposed cycle in Figure 17 shows a specific power division between both sub-systems so that all the produced brine be converted to sodium hypochlorite and hydrogen, Figure 18 shows the balanced proportion of power entered RO system and the mass flow rate of productions during a day. It has to be noted that the amount of power required for one kilogram *NaClO* production is about 3.5 kW [44]. It is noteworthy that this notion could be applied to the whole system water rejections which will discussed in the future studies.

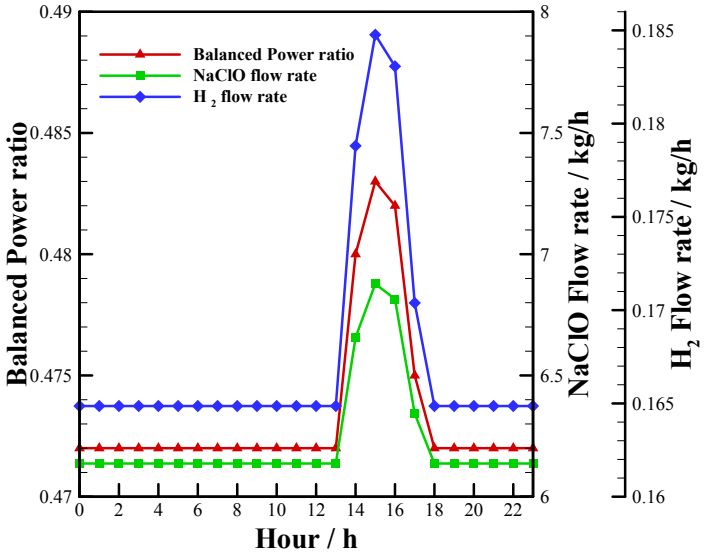

Figure 18 - Balanced power ratio, hydrogen and NaClO production rate.

4. Conclusion

In this study, utilization of a Stirling engine instead of a condenser in the solar-powered transcritical power cycle with the recovery of the cryogenic energy of liquefied natural gas is investigated for the hydrogen and permeate water production, simultaneously. A thermodynamic and exergy analysis is carried out to study the effect of employing Stirling engine between CO_2 power cycle and the LNG cycle to produce more electrical power within the system, and the effect of several key parameters on the overall performance of a system including permeate water and hydrogen production. Moreover, the cooperation of desalination and electrolyzer systems contributed to attaining an electrolyzer-based ZLD approach through the system. Several key conclusions of this study are as bellow:

An exergy analysis shows that the exergy mostly destructs in solar collectors and condenser of conventional CO_2 power cycle by about 42% and 16.7%, respectively. In comparison with conventional systems using a condenser, the exergy destruction through heat transfer from CO_2 to an LNG unit decreases by roughly half from 16.7% to 8.8%, for an ideal Stirling engine. So exergy destruction through the system decreased approximately 36.54 kW. The reduced exergy destruction interestingly converted to useful power within the Stirling engine leading to higher permeate and hydrogen production rate. The minimum power produced during the day by the ideal Stirling engine is noticeably at least 9 kW and 15 kW greater than CO_2 and LNG power productions. In other words, ideal Stirling engine produces more power than CO_2 and LNG power cycles. The exergy output of stream number 15 corresponding to the natural gas turbine output stream decreases due to a reduction in LNG mass flow rate of the system leading to lower heat transfer area within the LNG heater. An examination of some thermodynamic factors affecting the overall performance of the system shows that higher CO_2 turbine inlet pressure has an optimum producing fresh water and hydrogen, while the higher CO_2 turbine inlet temperature slightly reduced the productions rate. Furthermore, higher boiler inlet temperature and natural gas turbine inlet pressure provide more system output. The more recovery ratio causes a sharp reduction in hydrogen production. Meanwhile, it has an optimum amount of fresh water production at recovery ratio equals to 0.47. Employing electrolyzer beside desalination system to use highly concentrated brine stream of RO system would eliminate the wastewater rejection through proposed system leading to attaining a near-ZLD approach. Entering brine stream, wasting 2.58 kW of inlet exergy, to the Sodium Hypochlorite Generators leads to $NaClO$ production besides H_2 and removing brine disposal.

There are still further possible studies that could apply to this work in future research. An actual Stirling engine can thoroughly explore in the future works to find out the non-ideality effects on the system. Moreover, the ZLD notion could apply to whole proposed system.

References

[1] Chen, H., Goswami, D.Y. and Stefanakos, E.K., 2010. A review of thermodynamic cycles and working fluids for the conversion of low-grade heat. *Renewable and sustainable energy reviews*, *14*(9), pp.3059-3067. http://dx.doi.org/10.1016/j.rser.2010.07.006

[2] Sun, Z., Wang, J., Dai, Y. and Wang, J., 2012. Exergy analysis and optimization of a hydrogen production process by a solar-liquefied natural gas hybrid driven transcritical CO_2 power cycle. *International journal of hydrogen energy*, *37*(24), pp.18731-18739. http://dx.doi.org/10.1016/j.ijhydene.2012.08.028

[3] Kane, M., Larrain, D., Favrat, D. and Allani, Y., 2003. Small hybrid solar power system. *Energy*, *28*(14), pp.1427-1443. http://dx.doi.org/10.1016/S0360-5442(03)00127-0

[4] Boroojeni, K.G., Amini, M.H., Nejadpak, A., Iyengar, S.S., Hoseinzadeh, B. and Bak, C.L., 2016, May. A theoretical bilevel control scheme for power networks with large-scale penetration of distributed renewable resources. In *Electro Information Technology (EIT), 2016 IEEE International Conference on* (pp. 0510-0515). IEEE.

[5] Song, Y., Wang, J., Dai, Y. and Zhou, E., 2012. Thermodynamic analysis of a transcritical CO_2 power cycle driven by solar energy with liquified natural gas as its heat sink. *Applied energy*, *92*, pp.194-203. http://dx.doi.org/10.1016/j.apenergy.2011.10.021

[6] Xia, G., Sun, Q., Cao, X., Wang, J., Yu, Y. and Wang, L., 2014. Thermodynamic analysis and optimization of a solar-powered transcritical CO_2 (carbon dioxide) power cycle for reverse osmosis desalination based on the recovery of cryogenic energy of LNG (liquefied natural gas). *Energy*, *66*, pp.643-653. http://dx.doi.org/10.1016/j.energy.2013.12.029

[7] Cayer, E., Galanis, N., Desilets, M., Nesreddine, H. and Roy, P., 2009. Analysis of a carbon dioxide transcritical power cycle using a low temperature source. *Applied Energy*, *86*(7), pp.1055-1063. http://dx.doi.org/10.1016/j.apenergy.2008.09.018

[8] Cayer, E., Galanis, N. and Nesreddine, H., 2010. Parametric study and optimization of a transcritical power cycle using a low temperature source. *Applied Energy*, *87*(4), pp.1349-1357. http://dx.doi.org/10.1016/j.apenergy.2009.08.031

[9] Li, L., Ge, Y.T., Luo, X. and Tassou, S.A., 2016. Thermodynamic analysis and comparison between CO_2 transcritical power cycles and R245fa organic Rankine cycles for low grade heat to power energy conversion. *Applied Thermal Engineering*, *106*, pp.1290-1299. http://dx.doi.org/10.1016/j.applthermaleng.2017.01.024

[10] Ahmadi, M.H., Mehrpooya, M. and Pourfayaz, F., 2016. Exergoeconomic analysis and multi objective optimization of performance of a Carbon dioxide power cycle driven by geothermal energy with liquefied natural gas as its heat sink. *Energy Conversion and Management*, *119*, pp.422-434. http://dx.doi.org/10.1016/j.enconman.2016.04.062

[11] Ahmadi, M.H., Mehrpooya, M. and Pourfayaz, F., 2016. Thermodynamic and exergy analysis and optimization of a transcritical CO_2 power cycle driven by geothermal energy with liquefied natural gas as its heat sink. *Applied Thermal Engineering*, *109*, pp.640-652. http://dx.doi.org/10.1016/j.applthermaleng.2016.08.141

[12] Saadatfar, B., Fakhrai, R. and Fransson, T., 2014. Conceptual modeling of nano fluid ORC for solar thermal polygeneration. *Energy Procedia*, *57*, pp.2696-2705. https://doi.org/10.1016/j.egypro.2014.10.301

[13] Toghyani, S., Baniasadi, E. and Afshari, E., 2016. Thermodynamic analysis and optimization of an integrated Rankine power cycle and nano-fluid based parabolic trough solar collector. *Energy Conversion and Management*, *121*, pp.93-104. http://dx.doi.org/10.1016/j.enconman.2016.05.029

[14] Lin, W., Huang, M., He, H. and Gu, A., 2009. A transcritical CO_2 Rankine cycle with LNG cold energy utilization and liquefaction of CO_2 in gas turbine exhaust. *Journal of Energy Resources Technology*, *131*(4), p.042201.

[15] Angelino, G. and Invernizzi, C.M., 2009. Carbon dioxide power cycles using liquid natural gas as heat sink. *Applied Thermal Engineering*, *29*(14), pp.2935-2941. http://dx.doi.org/10.1016/j.applthermaleng.2009.03.003

[16] Mehrpooya, M., Kalhorzadeh, M. and Chahartaghi, M., 2016. Investigation of novel integrated air separation processes, cold energy recovery of liquefied natural gas and carbon dioxide power cycle. *Journal of Cleaner Production*, *113*, pp.411-425. http://dx.doi.org/10.1016/j.jclepro.2015.12.058

[17] Manolakos, D., Kosmadakis, G., Kyritsis, S. and Papadakis, G., 2009. On site experimental evaluation of a low-temperature solar organic Rankine cycle system for RO desalination. *Solar Energy*, *83*(5), pp.646-656. http://dx.doi.org/10.1016/j.solener.2008.10.014

[18] Manolakos, D., Kosmadakis, G., Kyritsis, S. and Papadakis, G., 2009. Identification of behaviour and evaluation of performance of small scale, low-temperature Organic Rankine Cycle system coupled with a RO desalination unit. *Energy*, *34*(6), pp.767-774. http://dx.doi.org/10.1016/j.energy.2009.02.008

[19] Manolakos, D., Papadakis, G., Kyritsis, S. and Bouzianas, K., 2007. Experimental evaluation of an autonomous low-temperature solar Rankine cycle system for reverse osmosis desalination. *Desalination*, *203*(1-3), pp.366-374. https://doi.org/10.1016/j.desal.2006.04.018

[20] Delgado-Torres, A.M. and García-Rodríguez, L., 2007. Status of solar thermal-driven reverse osmosis desalination. *Desalination*, *216*(1-3), pp.242-251. https://doi.org/10.1016/j.desal.2006.12.014

[21] Nafey, A.S., Sharaf, M.A. and García-Rodríguez, L., 2010. Thermo-economic analysis of a combined solar organic Rankine cycle-reverse osmosis desalination process with different

energy recovery configurations. *Desalination*, *261*(1), pp.138-147. http://dx.doi.org/10.1016/j.desal.2010.05.017

[22] Malek, A., Hawlader, M.N.A. and Ho, J.C., 1996. Design and economics of RO seawater desalination. *Desalination*, *105*(3), pp.245-261.https://doi.org/10.1016/0011-9164(96)00081-1

[23] Dincer, I., 2012. Green methods for hydrogen production. *International journal of hydrogen energy*, *37*(2), pp.1954-1971. http://dx.doi.org/10.1016/j.ijhydene.2011.03.173

[24] Ahmadi, P., Dincer, I. and Rosen, M.A., 2013. Energy and exergy analyses of hydrogen production via solar-boosted ocean thermal energy conversion and PEM electrolysis. *International Journal of Hydrogen Energy*, *38*(4), pp.1795-1805. http://dx.doi.org/10.1016/j.ijhydene.2012.11.025

[25] Dong, H., Zhao, L., Zhang, S., Wang, A. and Cai, J., 2013. Using cryogenic exergy of liquefied natural gas for electricity production with the Stirling cycle. *Energy*, *63*, pp.10-18. http://dx.doi.org/10.1016/j.energy.2013.10.063

[26] Szczygieł, I., Stanek, W. and Szargut, J., 2016. Application of the Stirling engine driven with cryogenic exergy of LNG (liquefied natural gas) for the production of electricity. *Energy*, *105*, pp.25-31. http://dx.doi.org/10.1016/j.energy.2015.08.112

[27] Szargut, J. and Szczygiel, I., 2009. Utilization of the cryogenic exergy of liquid natural gas (LNG) for the production of electricity. *Energy*, *34*(7), pp.827-837. http://dx.doi.org/10.1016/j.energy.2009.02.015

[28] Ahmadi, M.H., Sayyaadi, H., Dehghani, S. and Hosseinzade, H., 2013. Designing a solar powered Stirling heat engine based on multiple criteria: maximized thermal efficiency and power. *Energy Conversion and Management*, *75*, pp.282-291. http://dx.doi.org/10.1016/j.enconman.2013.06.025

[29] Ahmadi, M.H., Sayyaadi, H., Mohammadi, A.H. and Barranco-Jimenez, M.A., 2013. Thermo-economic multi-objective optimization of solar dish-Stirling engine by implementing evolutionary algorithm. *Energy Conversion and Management*, *73*, pp.370-380. http://dx.doi.org/10.1016/j.enconman.2013.05.031

[30] Ahmadi, M.H., Ahmadi, M.A., Mellit, A., Pourfayaz, F. and Feidt, M., 2016. Thermodynamic analysis and multi objective optimization of performance of solar dish Stirling engine by the centrality of entransy and entropy generation. *International Journal of Electrical Power & Energy Systems*, *78*, pp.88-95. http://dx.doi.org/10.1016/j.ijepes.2015.11.042

[31] Ahmadi, M.H., Ahmadi, M.A., Pourfayaz, F., Bidi, M., Hosseinzade, H. and Feidt, M., 2016. Optimization of powered Stirling heat engine with finite speed thermodynamics. *Energy Conversion and Management*, *108*, pp.96-105. http://dx.doi.org/10.1016/j.enconman.2015.11.005

[32] Ahmadi, M.H., Ahmadi, M.A., Pourfayaz, F., Hosseinzade, H., Acıkkalp, E., Tlili, I. and Feidt, M., 2016. Designing a powered combined Otto and Stirling cycle power plant through multi-objective optimization approach. *Renewable and Sustainable Energy Reviews*, *62*, pp.585-595. http://dx.doi.org/10.1016/j.rser.2016.05.034

[33] Lemmon, E.W., Huber, M.L. and McLinden, M.O., 2007. NIST thermodynamic and transport properties of refrigerants and refrigerant mixtures (REFPROP) version 8.0.

[34] Kalogirou, S.A., 2014. Solar Energy Collectors, in Solar Energy Engineering (Second Edition), Academic Press: Boston. p. 125-220. http://dx.doi.org/10.1016/B978-0-12-397270-5.00002-9

[35] Duffie, J.A. and Beckman, W.A., 1980. Solar engineering of thermal processes.

[36] Sukhatme, K. and S.P. Sukhatme, 1996. Solar Energy: Principles of Thermal Collection and Storage, Tata McGraw-Hill.

[37] Possamai, D.G. and Tapia, G.I.M., 2011. Thermodynamics Analysis of Stirling Engine.

[38] El-Dessouky, H.T. and H.M. Ettouney, 2002. Reverse Osmosis, in Fundamentals of Salt Water Desalination, Elsevier Science B.V.: Amsterdam. p. 409-437.

[39] Dincer, I. and Rosen, M.A., 2012. Exergy: energy, environment and sustainable development. Newnes.

[40] Ahmadi, P., Dincer, I. and Rosen, M.A., 2011. Exergy, exergoeconomic and environmental analyses and evolutionary algorithm based multi-objective optimization of combined cycle power plants. *Energy*, *36*(10), pp.5886-5898. http://dx.doi.org/10.1016/j.energy.2011.08.034

[41] Hepbasli, A., 2008. A key review on exergetic analysis and assessment of renewable energy resources for a sustainable future. *Renewable and sustainable energy reviews*, *12*(3), pp.593-661. http://dx.doi.org/10.1016/j.rser.2006.10.001

[42] Renewable energy organization of IRAN (SANA), Database for solar irradiation, http://www.suna.org.ir. (Accessed 15.12.1).

[43] Barrington, D.J. and Ho, G., 2014. Towards zero liquid discharge: the use of water auditing to identify water conservation measures. *Journal of Cleaner Production*, *66*, pp.571-576. http://dx.doi.org/10.1016/j.jclepro.2013.11.065.

[44] Sodium hypochlorite generation systems, http://www.denora.com/mrkets-products/electrolyzers/clortec.html, (Accessed 17.02.25).